Acta Metallurgica Vol 28, pp. 1315 to 1332

0001-6160/80/1001-1315$02.00/0

OVERVIEW NO. 9

PLASTIC CREEP FLOW EFFECTS IN THE DIFFUSIVE CAVITATION OF GRAIN BOUNDARIES

A. NEEDLEMAN and J. R. RICE

Division of Engineering, Brown University, Providence, RI 02912, U.S.A.

(*Received* 15 *January* 1980)

Abstract—We analyze the growth of cavities along grain interfaces by the combined processes of grain boundary diffusion and plastic dislocation creep in the adjoining grains. It is shown that the coupling between the processes can be expressed in terms of a parameter L, which has the dimensions of length and which is a function of material properties, temperature and applied stress; L decreases with increasing temperature and stress and has, e.g., values in the range of 0.25 to 25 μm for various pure metals when stressed to $10^{-3}\times$ shear modulus at 0.5 T_m. The contribution of dislocation creep to the cavity growth rate is shown to be negligible when L is comparable to or larger than the cavity spacing, but significant interactions occur, leading to growth rates very much in excess of those predicted on the basis of boundary diffusion alone, when L is comparable to or smaller than the cavity size. The coupling occurs because extensive dislocation creep allows local accommodation of matter diffused into the grain boundary from the cavity walls.

The cavity growth rate is analyzed by formulating a new variational principle that governs combined processes of grain boundary diffusion and non-linear viscous creep, and by implementing this principle through the finite-element method to obtain numerical solutions. Results for the cavity growth rate are presented for a wide range of ratios of L to cavity spacing, and of cavity radius to spacing. Also, results are presented for the total growth time of cavities from an initial size to final coalescence.

Résumé—Nous analysons la croissance de cavités intergranulaires par combinaison de la diffusion intergranulaire et du fluage de dislocations dans des grains adjacents. Nous montrons que le couplage entre les deux phénomènes peut s'exprimer à l'aide d'un paramètre L, qui a les dimensions d'une longueur et qui est fonction des propriétés du matériau, de la température et de la contrainte appliquée; L décroit lorsqu'on augmente la température ou la contrainte, et ses valeurs sont, par exemple, comprises entre 0,25 et 25 μm pour divers métaux purs soumis à une contrainte de $10^{3}\times$ le module de cisaillement à 0,5 T_f. Nous montrons que la contribution du fluage de dislocations à la vitesse de croissance des cavités est négligeable lorsque L est comparable ou supérieur à l'espacement des cavités, mais que, lorsque L est comparable ou inférieur à la taille des cavités, des interactions notables se produisent et conduisent à des vitesses de croissance nettement supérieures à celles qu'on prévoit en considérant la diffusion intergranulaire seule. Le couplage se produit, car un fluage de dislocations important permet une accommodation locale de la matière ayant diffusé dans les joints á partir des parois de cavités.

Nous analysons la vitesse de croissance des cavités en formulant un nouveau principe variationnel combinant les phénomènes de diffusion intergranulaire et de fluage visqueux non linéaire, et en appliquant ce principe à l'aide de la méthode des éléments finis pour obtenir les solutions numériques. Nous présentons les résultats sur la vitesse de croissance des cavités, pour un large domaine de rapports de L à l'espacement des cavités, et du rayon des cavités à leur espacement. Nous présentons également des résultats concernant le temps de croissance total des cavités depuis une taille initiale jusqu'á la coalescence finale.

Zusammenfassung—Wir analysieren das Wachstum von Hohlräumen entlang von Korngrenzen über die kombinierten Prozesse der Korngrenzdiffusion und des plastischen Versetzungskriechens in den angrenzenden Körnern. Es wird gezeigt, daß die Kopplung zwischen diesen Prozessen mit einem Parameter L beschrieben werden kann, der die Dimension einer Länge hat und der von Materialeigenschaften, Temperatur und angelegter Spannung abhängt. L nimmt ab mit ansteigender Temperatur und ansteigender Spannung und beträgt z.B. 0,25 bis 25 μm für verschiedene reine Metalle bei Scherbelastung von $10^{-3}\times$ Schermodul bei 0,5 T_m. Der Beitrag des Versetzungskriechens zur Hohlraumwachstumsrate ist -wie gezeigt wird- vernachlässigbar, wenn L vergleichbar oder größer ist als der Abstand zwischen den Hohlräumen. Wenn L jedoch vergleichbar oder kleiner wird als die Hohlraumgröße, tritt beträchtliche Wechselwirkung auf mit der Folge von Wachstumsraten, die weit über die auf der Grundlage der Korngrenzdiffusion errechneten hinausgehen. Die Kopplung tritt auf, da ausgedehntes Versetzungskriechen die von den Hohlraumwänden in die Korngrenze diffundierte Materie lokal anpassen kann.

Die Hohlraumwachstumsrate wird analysiert mit einem neu formulierten Variationsprinzip, welches die kombinierten Prozesse der Korngrenzdiffusion und des nichtlinearen Fließens unfaßt, und welches mittels der Methode der finiten Elemente numerische Lösungen ergibt. Ergebnisse für Hohlraumwachstumsraten werden für einen weiten Bereich des Verhältnisses zwischen L und Hohlraumabstand und zwischen Hohlraumdurchmesser und Abstand angegeben. Ebenso werden Ergebnisse vorgelegt für die totale Wachstumszeit von der anfänglichen Größe bis zum Zusammenwachsen.

1. INTRODUCTION

Processes of grain boundary cavitation, by diffusive motion of matter from cavity walls into the grain interface, have been studied extensively as a model for rupture at elevated temperature. The basic model for this process was introduced by Hull and Rimmer [1] and modified in various ways to account for boundary conditions [2, 3], non-equilibrium shapes of the rupture cavities [4, 5] and elastic deformations of the adjoining grains [6, 7].

However, the works mentioned neglect the influence of plastic creep flow on the diffusive cavitation process. Our aim here is to model the combined effects of diffusion *and* creep flow on cavity growth. As will be seen, at stress levels of the order $10^{-3}\,\mu$ and higher (μ = shear modulus) at $0.5\,T_m$ (T_m = melting temperature) interactions between diffusive transport and creep flow are typically very important, although not at much lower stresses, of the order $10^{-4}\,\mu$ at this temperature. These combined effects lead to rates of cavity enlargement which can be appreciably greater than would be the case for either mechanism acting in isolation. Indeed, the possible importance of plastic creep flow to rupture at elevated temperature is suggested indirectly by the well-known Monkman-Grant [8] correlation, in which the product $\dot{\epsilon}_{ss}t_r$ ($\dot{\epsilon}_{ss}$ = steady state creep strain rate, t_r = rupture time) is sometimes found to vary only slightly over ranges of stress and temperature which correspond to large changes in both factors.

A previous attempt to model the combined effects of creep and diffusion on cavity growth was made by Beere and Speight [9]. Their model constitutes only a very rough approximation, and is based on the concept of each cavity being surrounded by a spherical shell of effectively non-creeping material, within which a Hull-Rimmer diffusive cavitation process takes place, with these shells being embedded in a matrix of uniformly creeping material. The model has been modified and extended by Edward and Ashby [10], who also give a comprehensive discussion of its predictions for various materials and conditions of stress and temperature. In contrast, our work attempts to solve exactly (with the help of a numerical finite-element solution) the coupled problem of creep and diffusion. We find some important differences, to be discussed, with this concept of a non-deforming shell, although the approximate models are found to exhibit the proper trends and incorporate the key dimensionless parameters describing the coupling.

The program of the paper is as follows: In the next section we discuss the Hull-Rimmer model and indicate, following a discussion by Rice [11], why plastic creep flow effects are expected to be important in modifying its predictions. Then we establish a new variational principle governing problems of coupled plastic creep flow and grain boundary diffusion (the final form of this principle, equation (46) to follow, for axisymmetric cavities was stated but not developed in [11]), and use this principle as the basis for a finite-element solution for the rate of cavity growth. We show that the coupling between creep and diffusion can be expressed in terms of a stress and temperature dependent material length scale L introduced by Rice [11], where

$$L = (\mathscr{D}\sigma_\infty/\dot{\epsilon}_\infty)^{1/3}. \tag{1}$$

Here σ_∞ is the remotely applied 'equivalent' tensile stress, $\dot{\epsilon}_\infty$ the associated creep strain rate, and $\mathscr{D} = D_b\delta_b\Omega/kT$ ($D_b\delta_b$ = grain boundary diffusion coefficient, Ω = atomic volume, kT = energy per atom measure of temperature). In particular $\mathscr{D}$ appears as the coefficient in the equation

$$\Omega J_b = \mathscr{D}\,\partial\sigma_n/\partial r \tag{2}$$

relating the volumetric rate of matter diffusion, ΩJ_b, along a grain boundary to the gradient, $\partial\sigma_n/\partial r$, of normal stress σ_n acting on that boundary. Numerical values of L are given for several materials as a function of stress and temperature in the last three columns of the upper portion of Table 1 (to be discussed subsequently). When the length L is large (e.g., low σ and T) compared to cavity radius (a) and half-spacing (b), plastic creep flow effects can be neglected. On the other hand, at higher σ and T, when L is small compared to the spacing, coupled creep-diffusion effects are important and the ratio of cavity growth rate $\dot{a}$ to the prediction based on the rigid-grains (Hull–Rimmer) model is found to be a rapidly increasing function of the ratio a/L. In the limit of very large a/L, grain boundary diffusion makes no contribution to the growth rate. These conclusions are consistent with the models of Beere and Speight [9] and Edward and Ashby [10]. Indeed, for power-law creeping materials ($\dot{\epsilon} \propto \sigma^n$). Edward and Ashby show that the predicted strain to rupture in their approximate model depends, for a given initial a/b ratio, on material parameters only through a dimensionless grouping P where, in our notation,

$$P = \frac{1}{10}\left(\frac{4L^3}{b^3}\right)^{2/n} \tag{3}$$

They observe that for $P \geqslant 1$ (i.e., large values of our length parameter L or small cavity spacings b), there is a negligible contribution of creep flow to growth and rupture is controlled by grain boundary diffusion; for $P \lesssim 10^{-3}$, they suggest that grain boundary diffusion is negligible and rupture is controlled, essentially, by creep flow alone.

2. HULL–RIMMER MODEL AND MODIFICATIONS DUE TO PLASTIC CREEP FLOW

The Hull-Rimmer [1] model for diffusive cavity growth on a grain boundary is illustrated in Fig. 1, for the typical case [5] when the dominant mechanisms of matter transport are by surface and grain boundary diffusion. Two important assumptions are made in this model: First, surface diffusion is presumed to be

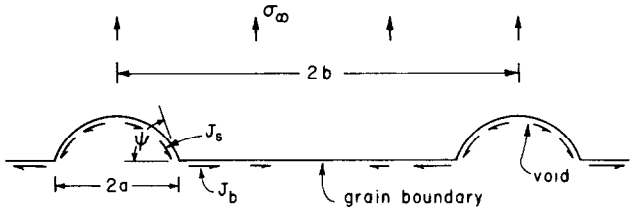

Fig. 1. Hull–Rimmer model for grain boundary cavitation by surface and grain boundary diffusion. The adjoining grains are assumed to separate as rigid bodies in this model.

rapid enough so that the void retains a quasi-equilibrium spherical-caps shape. (See Chuang *et al.* [5] for an analysis of conditions under which this assumption is valid, and for solutions to more general versions of the Hull-Rimmer model when the cavity has a non-equilibrium shape). Second, the grains are assumed to be effectively rigid (i.e., non-deforming). This means that the grains move apart uniformly as rigid bodies, hence requiring that matter be carried by diffusion along the entire segments of grain boundary between voids in order for cavity growth to occur.

Consideration of the *elastic* deformability of the adjoining grains suggests that this is relatively unimportant to modifying predictions of the model. Elastic effects are, of course, important in establishing the time scale required, after sudden load application, for attaining the quasi-steady conditions imagined in the model [11, 5]. Also, they are important for determining the transient concentrated stress fields that exist near the cavity tip when sudden increases of load occur [12]. But elastic strains are so small in representative cases that, once quasi-steady conditions are established, they can hardly modify the requirement that the grains move apart as effectively rigid bodies.

However, if the grains are stressed to a level for which extensive plastic creep flow occurs, grain deformability can, as we show, be considerably more important, leading to much faster cavity growth rates than predicted by the rigid-grains model. We assume that surface diffusion is sufficiently rapid to maintain the quasi-equilibrium, spherical-caps cavity shape. Considerations of [5] suggest that this will typically, but not always, be the case when the grains are modelled as rigid; the range of validity of this assumption remains an open issue for the present case of plastically creeping grains. Within this assumption, the physical processes which control the rate of cavity growth are grain boundary diffusion and plastic creep flow.

Figure 2 illustrates the ways in which creep flow can contribute to growth. We enumerate three regimes of response:

1. Consider first the case in which stresses are high and creep flow is sufficiently rapid that, as a limiting case, we may neglect matter transport along the grain boundary. The cavity growth rate for this case is discussed by Hancock [13]. As illustrated in Fig. 2a, the material points immediately adjacent to the void wall take on a distribution of velocities which tend to make the void increase in volume and, in general, under uniaxial tension and for widely-spaced voids (so that plastic creep flow is not concentrated in a voided layer along the grain boundary [10]), *decrease* in radius. This change in size and shape is indicated schematically by the dashed curve in Fig. 2a. But when surface diffusion is rapid, as we assume, local

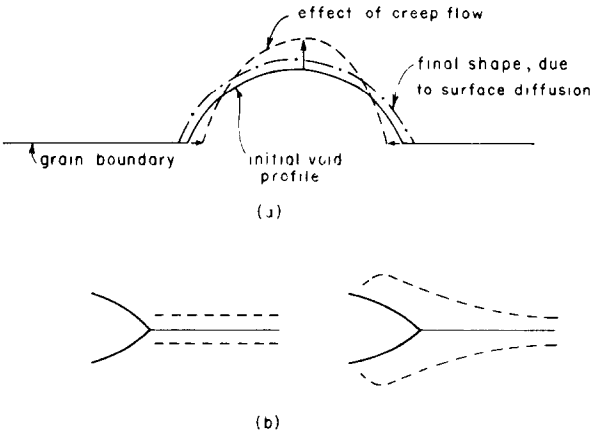

Fig. 2. Illustration of the effects of plastic creep flow. (a) Cavity growth by the combination of plastic creep flow (which, if considered alone, generally tends to decrease the void radius, dashed curve) and rapid surface diffusion; (b) Local accommodation of matter diffused into the grain boundary, by the deformation of grains. Note that the inscribed (dashed) lines do not remain straight as in the rigid-grains model. Thus, the diffusion path necessary to accommodate a given amount of matter is shorter.

matter transport along the void surface always serves to retain the quasi-equilibrium, spherical-caps shape (dash-dot-dash curve in Fig. 2a) so that the net effect is to *increase* the void radius.

The void volume may be written as

$$V = \frac{4\pi}{3} h(\psi) a^3 \tag{4}$$

where $h(\psi)$ is a function of the angle ψ which the void surface makes with the plane of the grain boundary at its tip. From [5],

$$h(\psi) = \left(\frac{1}{1 + \cos\psi} - \frac{\cos\psi}{2} \right) \sin\psi \,; \cos\psi = \gamma_b / 2\gamma_s. \tag{5}$$

For example $\psi = 70°$ is representative, and $h(70°) = 0.61$; of course, $h(90°) = 1$. Now, if $\dot{V}_{cr}$ is the rate of void volume enlargement due to creep flow (i.e., due to a velocity distribution immediately adjacent to the cavity surface associated with the dashed curve in Fig. 2a), then [11]

$$\frac{d}{dt}\left[\frac{4\pi}{3} h(\psi) a^3 \right] = \dot{V}_{cr}, \text{ or } h(\psi)\dot{a} = \dot{V}_{cr}/4\pi a^2. \tag{6}$$

For the case of a linear viscous material, $\dot{V}_{cr}$ may be evaluated from classical creeping flow solutions for axi-symmetric ellipsoidal cavities under uniaxial tension (results may be taken from elasticity solutions [14], replacing Poisson's ratio by 1/2 and the remote tensile strain ϵ_∞ by the remote tensile strain rate $\dot{\epsilon}_\infty$). The results for the limiting cases of spherical voids ($\psi = 90°$) and flat penny-shaped cracks ($\psi = 0$) are

$$\text{sphere: } \dot{V}_{cr} = \pi \dot{\epsilon}_\infty a^3; \quad \text{crack: } \dot{V}_{cr} = 4\dot{\epsilon}_\infty a^3. \tag{7}$$

The results are not very different, suggesting only a mild dependence on ψ, and we use the result for a sphere. Hence, using equation (6), the growth rate of widely-spaced voids is given by

$$h(\psi)\dot{a} \approx \dot{\epsilon}_\infty a/4 \tag{8}$$

in the present case for which there has been assumed to be negligible grain boundary diffusion. We assume for purposes of this discussion that (8) is approximately valid for non-linear power law creeping materials (only the numerical factor 1/4 could vary).

2. Assume now that both the processes of creep flow *and* grain boundary diffusion are active. This is a difficult case to analyze, and the remaining sections of the paper are devoted to it. It is important because we find that when both processes act simultaneously the cavity growth rate can be many times greater than would be the case of either mechanism acted in isolation. The reason for this is illustrated in Fig. 2b. On the left is shown the void at one instant in the growth history, and two straight lines (dashed lines in the figure) have been inscribed on the grains parallel to the boundary. On the right the void and the inscribed lines are shown after some amount of growth. Obviously, in the rigid-grains model the lines remain straight and matter must be transported along the entire grain boundary. But as remarked first by Beere and Speight [9], owing to plastic creep flow of the grains the matter can be accommodated locally, resulting in strong distortions of the inscribed lines as shown. Hence the path length over which matter must be diffused, to effect a given growth of the void, can be very much shorter than for the rigid-grains model. This means that less stress is required to effect the growth. Conversely, for a given stress level, the growth rate will be more rapid when local accommodation of the diffused matter is possible by creep. The sketch in Fig. 2b suggests rather strong effects of creep flow in the region of accommodation, and this raises some uncertainty about the concept of a shell of non-creeping material adjacent to the cavity [9, 10].

3. As a final case, assume that grain boundary diffusion is the dominant mechanism and that there is negligible creep flow. This is the Hull-Rimmer case, in which the grains are effectively rigid. Now the spacing 2b (Fig. 1) between voids is essential to the result, and we adopt the accepted approximation of considering the diffusion process to take place in an axially symmetric manner with the radial flux J_b along the grain boundary vanishing at a radius equal to b. That is, each void is effectively assumed to be centered in a right-circular cylinder of radius b (Fig. 3) with J_b vanishing at the outer radius. In this case the growth rate under remotely applies stress σ_∞ is [5]:

$$h(\psi)\dot{a} = \frac{\mathscr{D}[\sigma_\infty - (1 - a^2/b^2)\sigma_0]}{2a^2[\ln(b/a) - (3 - a^2/b^2)\,(1 - a^2/b^2)/4]}. \tag{9}$$

where $\mathscr{D}$ is defined in the text after equation (1) and where σ_0 is the normal stress acting on the grain boundary at the void tip,

$$\sigma_0 = \gamma_s(\kappa_1 + \kappa_2) = 2\gamma_s \sin\psi/a \tag{10}$$

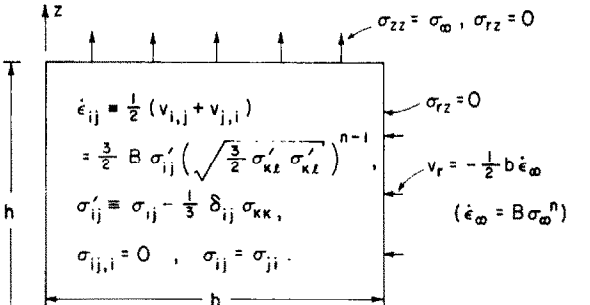

Fig. 3. Summary of the field equations and boundary conditions for the axisymmetric problem of combined plastic creep flow and grain boundary diffusion. The outer radius, b, of the cylinder represents the half-spacing between adjacent voids.

for a spherical-caps void. This value of σ_0 assures continuity of the chemical potential at the tip [5]; i.e., the potential per atom (neglecting strain energy terms, justifiably in representative cases [15]) is

$$\mu = -\gamma_s(\kappa_1 + \kappa_2)\Omega \tag{11}$$

on the cavity surface and

$$\mu = -\sigma_n\Omega \tag{12}$$

along the grain boundary, where σ_n is the local normal stress and Ω is the volume per atom. Equation (9) above for $\dot{a}$ actually corrects equation (71) of [5], which had an additional factor of $(1\text{-}a^2/b^2)$ on the right-hand side. Subsequently we will explain the origin of this error in the way that the condition of mass conservation was enforced. Related errors have been made in other work as well [16, 17], whereas, as pointed out in [16], the versions of equation (9) given in [1, 2] are incorrect because they are based on inappropriate boundary conditions. When $a^2/b^2 \ll 1$, the growth rate predicted by the rigid grains model is

$$h(\psi)\dot{a} = \mathscr{D}(\sigma_\infty - \sigma_0)/2a^2 \ln(b/2.12a). \tag{13}$$

Let $\dot{a}_{rg}$ be the growth rate predicted by (13) in the rigid grain case, regime 3, and $\dot{a}_{cr}$ be the rate predicted by (8) for regime 1 when creep is dominant and there is negligible contribution from grain boundary diffusion. Taking their ratio and recalling the definition of the temperature and stress level dependent parameter L, equation (1), we obtain [11]

$$\frac{\dot{a}_{cr}}{\dot{a}_{rg}} = \frac{\ln(b/2.12a)}{2(1-\sigma_0/\sigma_\infty)}\left(\frac{a}{L}\right)^3 \approx \left(\frac{a}{L}\right)^3 \tag{14}$$

(the factor multiplying $(a/L)^3$ ranges from 0.8 to 2.2 for b/a between 10 and 20, and σ_0/σ_∞ between 0 and 1/2). This equation must be used with care because, as we have emphasized, in regime 2 when both *g.b.* diffusion and creep flow are active simultaneously, $\dot{a}$ exceeds *both* $\dot{a}_{rg}$ and $\dot{a}_{cr}$. Nevertheless, the equation suffices to show in an elementary way the importance of the ratio a/L to determining the regime of response, and we will see that this same ratio arises as an expression of the coupling between creep and diffusion in the subsequent analysis of regime 2. As suggested by (14), and as will be shown, creep flow alone (regime 1) is important at large values of a/L, diffusion alone at small a/L, and over a rather broad transition regime (say, $0.2 < a/L < 20$), both mechanisms combine to produce growth in excess (in fact, *very* much in excess for, say, $1 < a/L < 5$) than either mechanism acting in isolation.

To estimate L as a function of stress and temperature, we write

$$\mathscr{D} = \frac{D_b\delta_b\Omega}{kT} = \frac{D_{b0}\delta_b\Omega}{kT}\exp\left(-\frac{Q_b}{RT}\right) \tag{15}$$

and we write for power-law dislocation creep

$$\dot{\epsilon}_\infty = A\frac{D_v\mu b}{kT}\left(\frac{\sigma_\infty}{\mu}\right)^n = A\frac{D_{v0}\mu b}{kT}\left(\frac{\sigma_\infty}{\mu}\right)^n \exp\left(-\frac{Q_v}{RT}\right) \tag{16}$$

(subscript 'v' refers to volume, or lattice, diffusion). Hence we can write

$$L \equiv (\mathscr{D}\sigma_\infty/\dot{\epsilon}_\infty)^{1/3} = L_0 \exp\left(\kappa\frac{T_m}{T}\right)\left(\frac{10^{-3}\mu}{\sigma_\infty}\right)^{(n-1)/3} \tag{17}$$

where T_m is the melting temperature and L_0 and κ are constants expressible in terms of the various material parameters appearing in the expressions for $\mathscr{D}$ and $\dot{\epsilon}$. Using a recent tabulation of data by Frost and Ashby [18] for all these material parameters, we show values of n, κ and L_0 in the first three columns of the upper portion of Table 1. The last three columns show values of L at two stress levels, $10^{-4}\mu$ and $10^{-3}\mu$, for $T = 0.5\ T_m$, and at the stress level $10^{-4}\mu$ for $T = 0.8\ T_m$. (These values of L differ somewhat from those presented by Rice [11] based on an earlier tabulation of data by Ashby [22]; obviously, there are significant uncertainties in the material parameters presented in Table 1 and entries are not always consistent with a recent but less extensive tabulation of diffusion parameters in [5]).

Consider the temperature $T = 0.5\ T_m$ and suppose that a is in the range of 1 μm. Then for $\sigma_\infty = 10^{-3}\mu$ (2nd to last column of Table 1), the interaction between creep and diffusion will be significant in cavity growth for all the materials shown except silver and perhaps nickel and magnesium, because L is comparable to or smaller in size than a. But at the ten-fold smaller stress level of $10^{-4}\mu$ (3rd to last column of Table 1), L is much larger than a for all the materials shown except chromium and perhaps tungsten, and at this stress level plastic creep flow is generally unimportant in contributing to the rate of cavity growth. The last column of Table 1 may be compared to the third to last, to see the effect of increasing temperature from 0.5 T_m to 0.8 T_m at the stress level of $10^{-4}\mu$; evidently, L is greatly reduced in size and hence creep flow becomes important to cavity growth for many of the materials shown at the higher temperature.

These observations suggest that at 0.5 T_m and for very low stress levels representative of multi-year service in energy generating equipment, say $\sigma_\infty \approx 1$ to $3 \times 10^{-4}\mu$, L will be large compared to representative cavity sizes for most materials (still, the highest stress level of this range reduces L by about a factor of 4 from the values in the third to last column of Table 1). Hence generally, but not always, for such cases plastic creep flow is not expected to make significant contributions to cavity growth under sustained load; i.e., response usually corresponds to regime 3 so that the rigid grain model applies approximately. Exceptions may occur due to high local

Table 1. Values of $L \equiv (\mathscr{D}\sigma/\dot{\epsilon})^{1/3} = L_0 e^{\kappa T_m/T}[\mu/10^3\sigma]^{(n-1)/3}$

Material		n	κ	$L_0(\mu m)$	$L(\mu m)$ $T = 0.5T_m$, $\sigma = 10^{-4}\mu$	$L(\mu m)$ $T = 0.5\ T_m$, $\sigma = 10^{-3}\mu$	$L(\mu m)$ $T = 0.8\ T_m$, $\sigma = 10^{-4}\mu$
f.c.c.	nickel	4.6	3.90	2.57×10^{-3}	99	6.3	5.3
	copper	4.8	2.73	1.58×10^{-2}	69	3.7	8.8
	silver	4.3	3.07	5.33×10^{-2}	310	25	31
	alluminum	4.4	2.48	4.30×10^{-3}	8.3	0.61	1.3
	lead	5.0	2.85	5.83×10^{-3}	38	1.8	4.4
	γ-iron	4.5	2.44	2.43×10^{-2}	47	3.2	7.6
b.c.c.	tungsten	4.7	2.16	3.40×10^{-3}	4.4	0.26	0.87
	chromium	4.3	2.10	3.74×10^{-3}	3.1	0.25	0.65
	molybdenum	4.85	1.96	6.02×10^{-3}	5.8	0.30	1.3
	α-iron	6.9	1.69	1.23×10^{-2}	34	0.36	9.5
h.c.p	zinc	4.5	1.79	3.55×10^{-2}	19	1.3	5.1
	magnesium	5.0	1.85	1.44×10^{-1}	130	6.0	32

Data on which table is based (from tabulation by Frost and Ashby [18]):

Material		$\Omega(m^3) \times 10^{29}$	$b(m) \times 10^{10}$	T_m(K)	$D_{v0}\ (m^2/s) \times 10^5$	Q_v (kJ/mole)	$\delta_b D_{b0}\ (m^3/s) \times 10^{14}$	Q_b (kJ/mole)	A
f.c.c.	nickel	1.09	2.49	1726	19	284	0.35	115	3.0×10^6
	copper	1.18	2.56	1356	2.0	197	0.50	104	7.4×10^5
	silver	1.71	2.86	1234	4.4	185	0.45	90	3.2×10^2
	aluminum	1.66	2.86	933	17	142	5.0	84	3.4×10^6
	lead	3.03	3.49	600	14	109	8.0	66	2.5×10^8
	γ-iron	1.21	2.58	1810	1.8	270	7.5	159	4.3×10^5
b.c.c.	tungsten	1.59	2.74	3683	56	585	33	385	1.1×10^8
	chromium	1.20	2.50	2163	2.8	306	0.50	192	1.3×10^6
	molybdenum	1.53	2.73	2883	5.0	405	5.5	263	1.0×10^8
	α-iron	1.18	2.48	1810	20	251	110	174	7.0×10^{13}
h.c.p.	zinc	1.52	2.67	693	1.3	91.7	1.3	60.5	4.0×10^4
	magnesium	2.33	3.21	924	10	135	500	92	1.2×10^6

$$(L_0 = 10^{n-1}\,[\delta_b D_{b0}\Omega/AbD_{v0}]^{1/3},\ \kappa = (Q_v - Q_b)/3RT_m)$$

thermal stresses in start-up operations, to local stress concentrations at notches or macrocrack tips, or to transient effects at sliding grain boundaries following alterations in load level. In these cases as well as other high stress situations, representative e.g. of turbine blade operation or of certain metal forming processes, substantial interaction between creep flow and diffusion is expected as for regime 2 above, and the cavity growth rate may exceed greatly predictions of the rigid-grain model. It seems unlikely that regime 1, requiring $L \ll a$, will be encountered in practical cases except at very high stress levels and perhaps in the terminal joining of cavities.

The large values of L for silver in Table 1 suggest that plastic creep flow might not be expected to contribute to cavity growth in practical cases. This may be significant in terms of the observations by Goods and Nix [23, 24] that creep fracture results for silver polycrystals with pre-existing grain boundary voids could be rationalized in terms of a purely diffusional model of the rigid-grains type, modified as in [4, 5] to account for non-equilibrium cavity shapes. However, it must be cautioned that their high-stress creep data for silver [24], with $n \approx 9$, leads to $L_0 \approx 10^{-4}\ \mu$m and to values of L which are not always large for the σ_∞ and T values of their experiments. Also, copper exhibits large values of L compared to representative microstructural sizes, except at relatively high stress levels, and this is also a material for which correlation of creep rupture lifetimes in terms of diffusional models of the rigid-grains type has been possible [1, 5, 25]. Finally, Miller [26] has correlated crack growth in αFe by a diffusional model at stresses of the order $2 \times 10^{-4}\ \mu$ and $T = 0.54\ T_m$. For this range we estimate $L \approx 7\ \mu$m from Table 1; the value is not as large compared to the cavity radius (5 μm) in his experiments as would be expected, by our present considerations, to justify neglecting plastic creep flow.

3. VARIATIONAL PRINCIPLE FOR COMBINED PLASTIC CREEP FLOW AND GRAIN BOUNDARY DIFFUSION

Here we examine the equations governing combined processes of plastic creep flow and grain boundary diffusion in some generality. Our purpose is to establish a variational principle. We will apply the principle as the basis for a finite-element solution to the axially symmetric cavity growth model, Fig. 3, but the general version of the principle may be useful for a variety of other creep-diffusion processes (e.g., establishing overall constitutive relations for polycrystals).

The material of the grains is taken as incompressible and non-linear viscous, specifically of the power-law form

$$\sigma = \Lambda \dot{\epsilon}^{1/n} \tag{18}$$

in uniaxial tension where Λ and n are constants (compare equation 16). This is generalized to arbitrary stress and strain rate states by writing (with the summation convention)

$$\sigma_{ij} - \tfrac{1}{3}\delta_{ij}\sigma_{kk} = \tfrac{2}{3}\Lambda \dot{\epsilon}^{-(n-1)/n}\dot{\epsilon}_{ij} \tag{19}$$

where

$$\dot{\epsilon} = \sqrt{\tfrac{2}{3}\dot{\epsilon}_{ij}\dot{\epsilon}_{ij}},\ \dot{\epsilon}_{kk} = 0 \tag{20}$$

and the strain rates are given in terms of material velocities v_i (relative to cartesian coordinates x_1, x_2, x_3) by

$$2\dot{\epsilon}_{ij} = \partial v_i/\partial x_j + \partial v_j/\partial x_i. \tag{21}$$

Further, the stresses must satisfy the equilibrium equations

$$\partial \sigma_{ij}/\partial x_i = 0 \text{ in } V,\quad n_i\sigma_{ij} = T_j \text{ on } S_T \tag{22}$$

where V is the volume occupied by the grains, and where T_i the surface traction and n_i the unit outer normal on the part of the external boundary, S_T, where tractions are prescribed. Observe that the relations of σ_{ij} to $\dot{\epsilon}_{ij}$ are such that

$$\int_0^{\dot{\epsilon}_{kl}} \sigma_{ij}\, \mathrm{d}\dot{\epsilon}_{ij} = \Omega(\dot{\epsilon}_{kl}) = \frac{n}{1+n}\Lambda \dot{\epsilon}^{(1+n)/n}. \tag{23}$$

Our subsequent equations are valid for any relation between σ_{ij} and $\dot{\epsilon}_{ij}$ (e.g., anisotropic, not of a power law type) so long as the integral is path-independent in strain rate space and hence defines only a function Ω of the end-point strain rates.

The solution to the above set of equations is well-known to be equivalent to the variational principle

$$\delta F = 0 \quad \text{to first order in} \quad \delta v_i \tag{24}$$

(in fact, F is not only stationary but a global minimum) where F is the following functional, defined on the class of kinematically admissible velocity and strain rate fields (i.e., related to one another by (21), meeting $\dot{\epsilon}_{kk} = 0$, and with v_i taking on proper values on any part of S where velocity is prescribed):

$$F = \int_V \Omega(\dot{\epsilon}_{kl})\, \mathrm{d}V - \int_{S_T} T_i v_i\, \mathrm{d}S. \tag{25}$$

It is straightforward to show that this same principle also applies to a polycrystal with freely-sliding grain boundaries, in which case the admissible fields v_i may have tangential discontinuities (but not normal discontinuities, unless diffusion is considered) on A, where A denotes the collection of grain boundaries. Although we do not pursue the matter here, it is also possible to generalize the principle to grain boundary sliding with viscous resistance by adding a term

$$\int_A \omega(\Delta v_\alpha)\, \mathrm{d}A \tag{26}$$

to F. Here Greek subscripts have the range 1,2 and refer to a local set of cartesian coordinates in the *g.b.*, and it is assumed that the shear stresses τ_α acting on the boundary are related to local velocity discontinuities Δv_α in such a way that

$$\int_0^{\Delta v_\beta} \tau_\alpha\, \mathrm{d}(\Delta v_\alpha) = \omega(\Delta v_\beta). \tag{27}$$

Now assume that diffusion takes place along grain boundaries (which are assumed to support no shear stress). Choose the normal n_i on each side of a grain boundary to point into the adjoining material (opposite to the convention on S) and observe that $n_i^+ = -n_i^-$, where $+$, $-$ denote the two sides of the boundary. Then, if $j_\alpha = \Omega J_\alpha$ is the volumetric flux crossing unit length in the grain boundary, matter conservation requires that

$$\partial j_\alpha/\partial x_\alpha + \Delta v_n = 0 \quad \text{on} \quad A \tag{28}$$

where

$$\Delta v_n = (n_i v_i)^+ + (n_i v_i)^-. \tag{29}$$

Further, the linear, isotropic form of the kinetic relation for diffusion is

$$j_\alpha = \Omega J_\alpha = -\frac{D_b \delta_b}{kT}\frac{\partial \mu}{\partial x_\alpha} = \mathscr{D}\partial\sigma_n/\partial x_\alpha \quad \text{on} \quad A \tag{30}$$

where (12) for μ has been used and

$$\sigma_n = n_i\sigma_{ij}n_j \text{ (same on + and − sides).} \tag{31}$$

Note also that $n_i\sigma_{i\alpha} = 0$ (no shear stresses), and that along the collection of arcs Γ where grain boundaries meet free surfaces (e.g., along the cavity apex in Fig. 3), σ_n takes on prescribed values

$$\sigma_n = \sigma_0 \quad \text{along} \quad \Gamma \tag{32}$$

where $\sigma_o = \gamma_s(\kappa_1 + \kappa_2)$ for continuity of potential and κ_1, κ_2 are the principal curvatures of the free surfaces adjoining Γ. It is not required for validity of what follows that these free surfaces be at equilibrium vis-a-vis surface diffusion.

To establish a variational principle satisfied by the solution to the coupled equations of creep flow (in V) and diffusion (on A), we begin by observing that the true stress field satisfies identically the principle of virtual work (or of virtual velocities) in the form

$$\int_V \sigma_{ij}\dot{\epsilon}_{ij}^* \, dV = \int_{S_T} T_i v_i^* \, dS - \int_A \sigma_n \Delta v_n^* \, dA \tag{33}$$

where v_i^*, $\dot{\epsilon}_{ij}^*$ are arbitrary fields associated by (21), with v_i^* taking on arbitrary discontinuities on A but vanishing on any portion of S where v_i is prescribed. Let j_α^* be the flux field associated with Δv_n^* by (28); it does not matter for our purposes that only its derivatives, and not j_α^* itself, are uniquely determined. Note, however, that j_α^* (as well as the true field j_α) must satisfy a condition of the form

$$\Sigma(m_\alpha j_\alpha^*) = 0 \tag{34}$$

at junctions of grain boundaries, where the sum extends over each grain facet at the junction and m_α is the local normal to the arc of intersection, chosen to be directed *into* the plane of each participating grain facet.

We may write

$$\begin{aligned}\int_A \sigma_n \Delta v_n^* \, dA &= -\int_A \sigma_n \partial j_\alpha^*/\partial x_\alpha \, dA \\ &= \int_A \partial\sigma_n/\partial x_\alpha j_\alpha^* \, dA - \int_A \partial(\sigma_n j_\alpha^*)/\partial x_\alpha \, dA \\ &= \int_A \partial\sigma_n/\partial x_\alpha j_\alpha^* \, dA + \int_\Gamma \sigma_n m_\alpha j_\alpha^* \, d\Gamma \\ &= \int_A \frac{1}{\mathscr{D}} j_\alpha j_\alpha^* \, dA + \int_\Gamma \sigma_0 m_\alpha j_\alpha^* \, d\Gamma. \end{aligned} \tag{35}$$

Here, in the first equality we have used (28) for the * field; in the third we have applied the divergence theorem to the collection of grain boundary facets A (noting that (34) holds at all grain junctions and that, by continuity of the potential μ of (12) at such junctions, σ_n must be the same for every participating facet); in the last equality we have used (30) for $\partial\sigma_n/\partial x_\alpha$ and (32) for σ_n. When equation (35) is substituted into the principle of virtual work, equation (33), and we make the identifications

$$v_i^* = \delta v_i, \quad \dot{\epsilon}_{ij}^* = \delta\dot{\epsilon}_{ij}, \quad j_\alpha^* = \delta j_\alpha, \tag{36}$$

and further require that δv_i be such that $\delta\dot{\epsilon}_{kk} = 0$, we find that the solution to the coupled creep-diffusion problem satisfies the following variational principle:

$$\delta F = 0 \text{ to first order in } \delta v_i \tag{37}$$

where F is the functional defined by

$$\begin{aligned} F = &\int_V \Omega(\dot{\epsilon}_{kl}) \, dV - \int_{S_T} T_i v_i \, dS \\ &+ \int_A \frac{1}{2\mathscr{D}} j_\alpha j_\alpha \, dA + \int_\Gamma \sigma_0 m_\alpha j_\alpha \, d\Gamma \end{aligned} \tag{38}$$

for all kinematically associated fields v_i, $\dot{\epsilon}_{kl}$, j_α [i.e., satisfying equations (21) and (28) and chosen so that v_i takes on proper values at points of S where it is prescribed and that $\dot{\epsilon}_{kk} = 0$].

Conversely, by inverting the procedure of derivation, it is straightforward to show that the variational principle implies the full set of field equations that we have given and, also, that F is not only stationary but also a global minimum for the true field.

We note that the coupled problem that we have described has the feature that the current velocity field is fully determined by the current configuration of the body, by the current tractions T_i on S_T and by the current values assigned to σ_0 on Γ. In other words, there are no 'transient' effects associated with sudden loading of such a body (although the velocity field will change in time as the configuration changes, for example, by cavity growth).

4. AXIALLY SYMMETRIC CAVITY GROWTH MODEL AND FINITE ELEMENT FORMULATION

In Fig. 3 we show a spherical-caps cavity of radius a in a circular annulus of grain boundary of outer radius b. The adjoining grains are represented by right circular cylinders. The remotely acting tensile creep strain rate is $\dot{\epsilon}_\infty$, and the corresponding equivalent tensile stress is σ_∞ (i.e., $\sigma_\infty = A\dot{\epsilon}_\infty^{1/n}$). In general the latter will differ from the remotely applied tensile stress, $\sigma_{zz\infty}$, when there is triaxial stressing, and

$$\sigma_{zz\infty} = \sigma_\infty + \sigma_{rr\infty} \tag{39}$$

where $\sigma_{rr\infty}$ is the stress acting in the radial direction far from the cavitated grain boundary. (When $\sigma_{rr\infty}$ is non-zero, $\sigma_{zz\infty}$ should replace σ_∞ in equations (9) and (13) for the rigid-grains model). In order to simulate constraint of adjoining material, we take the radial velocity to be uniform at $r = b$, and hence the same as in the remote field. Thus the boundary conditions on the external surface are

$$\begin{aligned} &\text{On } z = h\text{: } T_z = \sigma_{zz\infty},\ T_r = 0 \\ &\text{On } r = b\text{: } T_z = 0,\ v_r = -\tfrac{1}{2}\dot{\epsilon}_\infty b \end{aligned} \tag{40}$$

and, of course, $T_r = T_z = 0$ on the cavity wall.

If $v_z(r, 0)$ is the vertical velocity along the grain boundary, the axially symmetric version of (28) is

$$\frac{1}{r}\frac{\partial}{\partial r}(rj) + 2v_z(r, 0) = 0 \tag{41}$$

where j is the radial matter flux, and when this equation is integrated subject to $j = 0$ at $r = b$ (since the outer boundary represents, approximately, a half spacing between cavities as in Fig. 1)

$$j = \frac{2}{r}\int_r^b r' v_z(r', 0)\, dr'. \tag{42}$$

We assume the power law stress-strain rate relation so that Ω is given by (23), and note that A of equations (18) and (23) can be written as $\sigma_\infty \dot{\epsilon}_\infty^{-1/n}$.

It is convenient to write the variational functional, F, in dimensionless form and to this end let $R = r/a$, $Z = z/a$, $B = b/a$, $H = h/a$, and define dimensionless velocities by

$$V_R(R,Z) = v_r(r,z)/\dot{\epsilon}_\infty a,\ V_Z(R,Z) = v_z(r,z)/\dot{\epsilon}_\infty a. \tag{43}$$

Then F is defined for all fields V_R, V_Z satisfying $V_R(B,Z) = -B/2$ and the condition of incompressibility,

$$\partial V_R/\partial R + V_R/R + \partial V_Z/\partial Z = 0. \tag{44}$$

Further, the dimensionless equivalent strain rate $\dot{E}$ $(= \dot{\epsilon}/\dot{\epsilon}_\infty)$ is defined in terms of V_R, V_Z by

$$\dot{E} = \left[\frac{2}{3}\left(\frac{\partial V_R}{\partial R}\right)^2 + \frac{2}{3}\left(\frac{V_R}{R}\right)^2 + \frac{2}{3}\left(\frac{\partial V_Z}{\partial Z}\right)^2 + \frac{1}{3}\left(\frac{\partial V_Z}{\partial R} + \frac{\partial V_R}{\partial Z}\right)^2\right]^{1/2}. \tag{45}$$

Thus, forming the functional F of (38) and recalling the definition of L in (1), we obtain the functional introduced by Rice in [11],

$$\begin{aligned} \frac{F}{4\pi\sigma_\infty\dot{\epsilon}_\infty a^3} = {} & \frac{n}{1+n}\int_0^H\int_{R_0(Z)}^B \dot{E}^{(1+n)/n} R\, dR\, dZ \\ & - \frac{\sigma_{zz\infty}}{\sigma_\infty}\int_0^B V_Z(R, H) R\, dR \\ & + \left(\frac{a}{L}\right)^3 \int_1^B \frac{1}{R}\left[\int_R^B R' V_Z(R', 0)\, dR'\right]^2 dR \\ & + \frac{\sigma_0}{\sigma_\infty}\int_1^B R' V_Z(R', 0)\, dR'. \end{aligned} \tag{46}$$

Here $R_0(Z)$ is the (dimensionless) cavity radius at height Z, for Z within the cavity height, and zero for larger values of Z. The form of this expression for F shows that a/L is the parameter which expresses the coupling between plastic creep flow and grain boundary diffusion.

A numerical solution to the governing equations, $\delta F = 0$, with F defined by (46), is obtained by means of the finite element method. The features of this boundary value problem which complicate the finite element formulation are: (i) the material incompressibility and non-linearity and (ii) the diffusional terms (the last two integrals in (46)). The method employed here, developed by Needleman and Shih [19], utilizes constant strain triangles arranged in a quadralateral mesh so that the sides of the triangles comprise the sides and diagonals of the quadralaterals. The incompressibility constraint is imposed on the admissible velocity fields by direct elimination of nodal degrees of freedom and the nonlinear variational equation is solved by the Newton-Raphson method. For axisymmetric problems, unlike for the plane strain problems on which attention was focused in [19], incompressibility is not satisfied pointwise within each element but in some average sense. However, numerical experiments show that the errors induced by employing the method of [19] to satisfy incompressibility approximately, rather than exactly, in axisymmetric problems is negligible for meshes with the relatively small elements that we employ (these errors are thought to be of the same order as those introduced by the discretization process itself). The finite element mesh employed here, for the case $b/a = 10.0$, is depicted in Fig. 4.

The diffusional terms in (46) are evaluated as follows; first we define

$$f(R) = \int_R^B R' V_Z(R', 0)\, dR' \tag{47}$$

and note that along $Z = 0$, V_Z is given by

$$V_Z(R, 0) = \sum_{i=1}^N W_i \phi_i(R). \tag{48}$$

Here, W_i are the nodal values of V_Z, N is the number

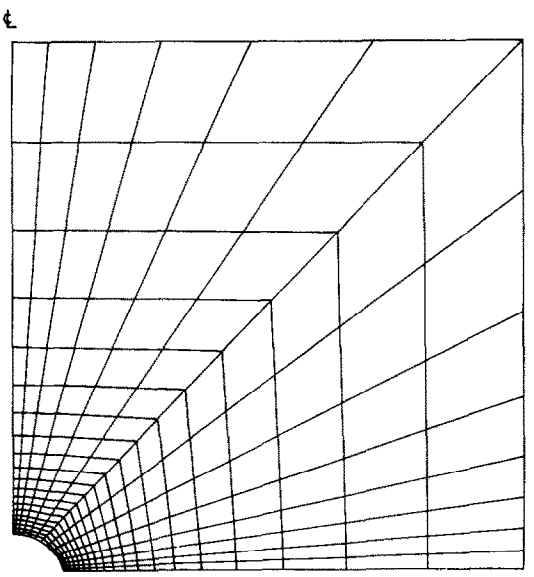

Fig. 4. Finite element mesh used for analyzing the problem outlined in Fig. 3 with $a/b = 0.1$. Each quadrilateral is composed of four triangles.

of nodes along the line $Z = 0$ and $\phi_i(R)$ is the 'hat' function,

$$\phi_i(R) = \begin{cases} \dfrac{R - R_{i-1}}{R_i - R_{i-1}} & R_{i-1} \leqslant R \leqslant R_i \\ \dfrac{R_{i+1} - R}{R_{i+1} - R_i} & R_i \leqslant R \leqslant R_{i+1} \\ 0 & R < R_{i-1} \quad \text{or} \quad R > R_{i+1} \end{cases} \tag{49}$$

Employing (48) in (47) enables $f(R)$ to be written as

$$f(R) = \sum_{i=1}^{N} W_i g_i(R) \tag{50}$$

where

$$g_i(R) = \int_R^B R' \phi_i(R')\, dR'. \tag{51}$$

The simple form of the 'hat' functions permits $g_i(R)$ to be evaluated analytically. The integral in (46) multiplying σ_0 is simply

$$\int_1^B R V_Z(R, 0)\, dR = \sum_{i=1}^{N} W_i g_i(1) \tag{52}$$

while the integral multiplying $(a/L)^3$ takes the form

$$\int_1^B \frac{1}{R} f^2(R)\, dR = \sum_{i=1}^{N} \sum_{j=1}^{N} K_{ij} W_i W_j \tag{53}$$

with

$$K_{ij} = \int_1^B \frac{1}{R} g_i(R) g_j(R)\, dR. \tag{54}$$

Since K_{ij} is obviously symmetric ($K_{ij} = K_{ji}$), only the elements of $\mathbf{K}$ for which say, $j \geqslant i$, need be evaluated. These can be written in one of three forms:

$$\begin{aligned} K_{ii} &= g_i^2(1) \ln R_{i-1} + \int_{R_{i-1}}^{R_{i+1}} \frac{g_i^2(R)}{R}\, dR \text{ (no sum on } i) \\ K_{i,i+1} &= g_i(1) g_{i+1}(1) \ln R_{i-1} \\ &\quad + \int_{R_{i-1}}^{R_{i+1}} \frac{g_i(R) g_{i+1}(R)}{R}\, dR \\ K_{ij} &= g_i(1) g_j(1) \ln R_{i-1} \\ &\quad + g_j(1) \int_{R_{i-1}}^{R_{i+1}} \frac{g_j(R)}{R}\, dR \quad (j > i+1) \end{aligned} \tag{55}$$

Each of the integrals remaining in (55) is evaluated by numerical integration; four Gaussian points being used in each of the subintervals $R_{i-1} \leqslant R \leqslant R_i$ and $R_i \leqslant R \leqslant R_{i+1}$. The finite element method described in [19] is then employed to descretize the remaining integrals in (46) and to solve the resulting nonlinear algebraic equations.

The results are presented following the discussion in the next section on the computation of the rate of cavity growth.

5. DETERMINATION OF THE RATE OF CAVITY GROWTH

The procedures of the last section lead to a determination of the velocity field v_r, v_z everywhere in the body and, by (42), the flux j along the boundary is determined also. To compute the rate of cavity growth we observe that since the material is incompressible, $\dot{V}$ must be equal to the net rate at which volume crosses an arbitrary surface surrounding the cavity. We can shrink this surface onto the cavity itself so that if A_c denotes the upper surface of the cavity and n_i is the normal to A_c, directed into the adjacent material,

$$\dot{V} = 2\pi a j_0 + 2 \int_{A_c} (n_r v_r + n_z v_z)\, dA. \tag{56}$$

Here v_r, v_z are velocities of material points immediately adjacent to the cavity wall (because of surface diffusion, these are *not* the same as dr/dt, dz/dt, where r,z are coordinates of the cavity wall) and j_0 is the grain boundary flux at the cavity tip,

$$j_0 = \frac{2}{a} \int_a^b r v_z(r, 0)\, dr \tag{57}$$

by (42). Thus, using (4) for $\dot{V}$ in the case when surface diffusion is rapid enough to retain the quasi-equilibrium cavity shape,

$$h(\psi)\dot{a} = \frac{j_0}{2a} + \frac{1}{2\pi a^2} \int_{A_c} (n_r v_r + n_z v_z)\, dA. \tag{58}$$

We digress to discuss the form of these equations in the rigid-grains case, for which the entire body of Fig. 3 has a uniform upward velocity v_z, with $v_r = 0$.

In previous treatments of this case the integral in equations (56) and (58) was neglected. It has the value $\pi a^2 v_z$ and hence

$$h(\psi)\dot{a} = j_0/2a + v_z/2, \tag{59}$$

while, from (57):

$$j_0 = v_z(b^2 - a^2)/a. \tag{60}$$

Thus

$$h(\psi)\dot{a} = j_0/2a(1 - a^2/b^2) = v_z b^2/2a^2. \tag{61}$$

In Refs [5, 16, 17] the term v_z in (59) was deleted, resulting in a deletion of the term $(1 - a^2/b^2)$ in the version of (61) in terms of j_0 [5], and an unwanted factor of $(1 - a^2/b^2)$ in the version of (61) in terms of v_z [16, 17]. This is the origin of the correction incorporated into (9). Fortunately, its effect is small since $(1 - a^2/b^2)$ differs little from unity over most of the growth range of practical interest.

Other minor differences remain in the final versions of the growth rate law, and these have to do with the way that different authors treat the surface tension, T_s (i.e., surface *stress*, as distinct from surface *energy*, γ_s). Chuang *et al.* [5] tacitly assume that $T_s = 0$ (as we do here also) whereas Raj and Ashby [16] and Raj *et al.* [17] assume $T_s = \gamma_s$. As Herring [20, 21] has remarked, there is no reason for either of the choices of T_s to be correct and, in fact, T_s may well be negative (surface compression) in many cases. The general result, when T_s exists, is given by replacing the term within brackets in the numerator of (9) by

$$[\sigma_\infty - (1 - a^2/b^2)2\gamma_s \sin\psi/a - (a^2/b^2)2T_s \sin\psi/a] \tag{62}$$

and, as noted, σ_∞ should be replaced by $\sigma_{zz\infty}$ when triaxial stresses are applied. Some authors give results in terms of the average stress $\bar{\sigma}$ acting over the unvoided portion of grain boundary, and in that case σ_∞ is to be replaced by $(1 - a^2/b^2)\bar{\sigma}$; this form is also valid if there is pressure acting inside the cavity [17]. (A recent analysis of surface tension effects by Rice and Chuang [15] suggests that continuity of μ at the tip, indeed, the avoidance of Dirac-like singularity in μ at the tip, can be satisfied only if surface strains are developed in such a way as to make T_s (and the corresponding grain boundary tension, T_b, vanish there).

Returning to the solution for creeping grains, the growth rates that we report are calculated from equations (58) and (57), using numerical results for the velocity field from the finite-element solution.

6. NUMERICAL RESULTS FOR CAVITY GROWTH RATES

Numerical solutions of the axisymmetric cavity growth model described in Section 4 were carried out for ratios of cavity radius to cavity half-spacing, a/b, of 1/10, 1/5, 1/3 and 2/3. The height, h, of the cylindrical region depicted in Fig. 3 was taken large enough ($h = 10a$ for $a/b = 1/10$ and $h = 5a$ for the remaining three values of a/b) to effectively eliminate any dependence of the solution on h. In all calculations the spherical cap tip equilibrium angle, ψ, was assumed to be 70° and the creep stress exponent, n, of the grains was taken to be 5. Values of a/L of $10^{j/2}$, $j = -4$ to 4, were chosen in order to explore the range from essentially rigid grains behavior to creep flow dominated behavior in equal intervals (of 0.5) of $\log_{10}(a/L)$.

Table 2. Cavity volumetric growth rates, $\dot{V}$, for a cavity radius to cavity half-spacing ratio, a/b, of 1/10

a/L	σ_0/σ_∞	$\dot{V}/\dot{\epsilon}_\infty a^3$	$\dot{V}/\dot{V}_{RG}$
0.01	1.0	4.02×10^4	1.00
0.0316	1.0	1.30×10^3	1.02
0.1	1.0	65.1	1.62
0.316	1.0	20.1	15.8
1.0	1.0	10.2	2.54×10^2
3.16	1.0	6.30	4.94×10^3
10.0	1.0	5.10	1.27×10^5
0.01	0.5	—	—
0.0316	0.5	6.43×10^4	1.00
0.1	0.5	2.12×10^3	1.04
0.316	0.5	1.20×10^2	1.88
1.0	0.5	18.8	9.27
3.16	0.5	7.33	1.14×10^2
10.0	0.5	5.23	2.58×10^3
0.01	0.0	4.02×10^6	1.00
0.0316	0.0	1.27×10^5	1.00
0.1	0.0	4.17×10^3	1.04
0.316	0.0	2.19×10^2	1.72
1.0	0.0	27.3	6.79
3.16	0.0	8.38	65.9
10.0	0.0	5.34	1.33×10^3

Numerical results for values of σ_0/σ_∞, the ratio of the normal stress acting on the grain boundary at the void tip to the remotely applied stress, of 0.0, 0.5 and 1.0 are displayed in Tables 2 to 5. The non-

Table 3. Cavity volumetric growth rates, $\dot{V}$, for a cavity radius to cavity half-spacing, a/b, of 1/5

a/L	$\sigma_0\sigma_\infty$	$\dot{V}/\dot{\epsilon}_\infty a^3$	$\dot{V}/\dot{V}_{RG}$
0.01	1.0	2.80×10^5	1.00
0.0316	1.0	8.86×10^3	1.00
0.1	1.0	2.95×10^2	1.06
0.316	1.0	23.5	2.66
1.0	1.0	10.3	36.8
3.16	1.0	6.32	7.15×10^2
10.0	1.0	5.13	1.84×10^4
0.01	0.5	—	—
0.0316	0.5	1.15×10^5	1.00
0.1	0.5	3.66×10^3	1.01
0.316	0.5	1.43×10^2	1.25
1.0	0.5	19.0	5.23
3.16	0.5	7.35	64.0
10.0	0.5	5.24	1.44×10^3
0.01	0.0	7.00×10^6	1.00
0.0316	0.0	—	—
0.1	0.0	7.03×10^3	1.01
0.316	0.0	2.61×10^2	1.18
1.0	0.0	27.6	3.95
3.16	0.0	8.40	38.0
10.0	0.0	5.34	7.46×10^2

Table 4. Cavity volumetric growth rates, $\dot{V}$, for a cavity radius to cavity half-spacing ratio, a/b, of 1/3

a/L	σ_0/σ_∞	$\dot{V}/\dot{\epsilon}_\infty a^3$	$\dot{V}/\dot{V}_{RG}$
0.01	1.0	1.53×10^6	1.00
0.0316	1.0	—	—
0.1	1.0	1.54×10^3	1.01
0.316	1.0	58.6	1.21
1.0	1.0	10.8	7.06
3.16	1.0	6.29	1.30×10^2
10.0	1.0	5.03	3.29×10^3
0.01	0.5	—	—
0.0316	0.5	2.42×10^5	1.00
0.1	0.5	7.66×10^3	1.00
0.316	0.5	2.56×10^2	1.06
1.0	0.5	20.2	2.64
3.16	0.5	7.34	30.4
10.0	0.5	5.16	6.75×10^2
0.01	0.0	1.38×10^7	1.00
0.0316	0.0	—	—
0.1	0.0	1.38×10^4	1.00
0.316	0.0	4.54×10^2	1.04
1.0	0.0	29.5	2.14
3.16	0.0	8.40	19.3
10.0	0.0	5.30	3.85×10^2

dimensionalized cavity volumetric growth rate, $\dot{V}/\dot{\epsilon}_\infty a^3$, was calculated from (56) using numerical integration. For comparison purposes the ratios of the calculated cavity growth rates, $\dot{V}$, to the corresponding growth rates obtained employing the rigid grains model, $\dot{V}_{RG}$, are also tabulated. Blank entries in Tables 2 to 5 correspond to cases, not computed, for which $\dot{V}/\dot{V}_{RG}$ is clearly unity.

For small values of a/L, how small depending on a/b and σ_0/σ_∞, the numerically computed growth rates coincide with those given by the rigid grains model, while for large a/L the numerically computed growth rates are approaching an asymptotic value appropriate for the purely plastic creep flow case. At fixed a/L, the ratio $\dot{V}/\dot{V}_{RG}$ increases with decreasing a/b and with increasing σ_0/σ_∞. For example, taking $a/L = 0.1$, with $a/b = 1/10$ and $\sigma_0/\sigma_\infty = 1.0$, the calculated volumetric growth rate is 62% greater than given by the rigid grains model while with $a/b = 1/3$, $a/L = 0.1$ and $\sigma_0/\sigma_\infty = 1.0$, the computed volumetric growth rate is only 1% above the prediction of the rigid grain model. With $a/L = 0.1$ and $a/b = 1/10$, increasing σ_0/σ_∞ from 0.0 to 1.0, increases $\dot{V}/\dot{V}_{RG}$ from 1.04 to 1.62, although, of course, the magnitude of $\dot{V}$ decreases with increasing σ_0/σ_∞.

The enhancement of the computed cavity volumetric growth rates over those given by the rigid grains model arises from the plastic deformation of the grains which permits matter to be accommodated locally near the void tip as illustrated in Fig. 2b. This reduces the diffusive path length and, hence, permits a more rapid removal of matter from the cavity wall than can take place in the rigid grains model. Figs. 5 to 7, illustrate this accommodation, for increasing values of a/L, with $a/b = 1/10$ and $\sigma_0/\sigma_\infty = 0.5$. Plotted in these figures is the distribution of the normal velocity along the grain boundary, which is half the separational velocity of the grains. Also shown in these figures are the corresponding values of the normal velocity in the rigid grains model. Obviously, in the rigid grains model the normal velocity along the grain boundary is constant. For a/L less than 0.1, not shown here, the computed normal velocity along the grain boundary is essentially constant and coincides with that given by the rigid grains model. For $a/L = 0.1$, there is significant local accommodation in the grains, however most of the cavity growth rate is still due to the translational separation of the grains. As illustrated in Figs. 6 and 7 when a/L increases the deformation that takes place to accommodate the

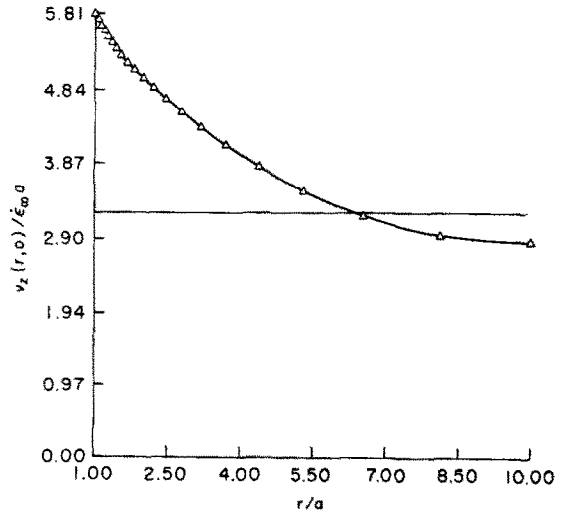

Fig. 5. The vertical velocity distribution (half the separational velocity of the grains) along the grain boundary for $a/b = 0.1$, $a/L = 0.1$ and $\sigma_0/\sigma_\infty = 0.5$. The triangles show the computed nodal values and the straight line is the distribution according to the rigid grains model.

Table 5. Cavity volumetric growth rates, $\dot{V}$ for a cavity radius to cavity half-spacing ratio, a/b, of 2/3.

a/L	σ_0/σ_∞	$\dot{V}/\dot{\epsilon}_\infty a^3$	$\dot{V}/\dot{V}_{RG}$
0.01	1.0	—	—
0.316	1.0	—	—
0.1	1.0	5.53×10^4	1.00
0.316	1.0	1.76×10^3	1.01
1.0	1.0	63.8	1.15
3.16	1.0	9.81	5.61
10.0	1.0	7.10	1.28×10^2
0.01	0.5	—	—
0.0316	0.5	—	—
0.1	0.5	8.98×10^4	1.00
0.316	0.5	2.85×10^3	1.00
1.0	0.5	99.3	1.11
3.16	0.5	11.6	4.08
10.0	0.5	7.28	81.1
0.01	0.0	—	—
0.0316	0.0	—	—
0.1	0.0	1.24×10^5	1.00
0.316	0.0	3.94×10^3	1.00
1.0	0.0	1.35×10^2	1.09
3.16	0.0	13.6	3.46
10.0	0.0	7.48	6.02

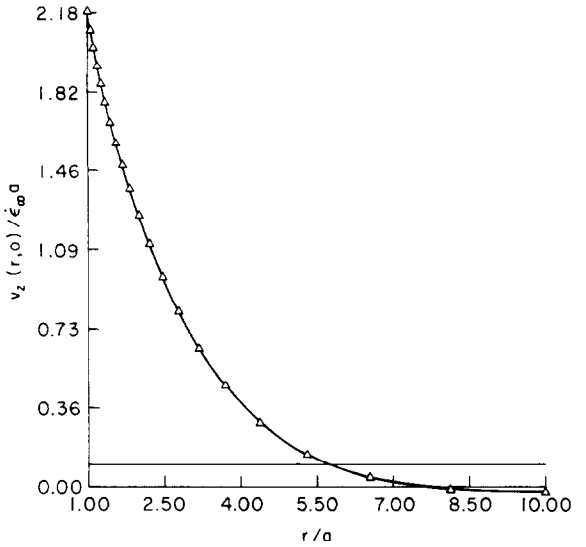

Fig. 6. The vertical velocity distribution (half the separational velocity of the grains) along the grain boundary for $a/b = 0.1$, $a/L = 0.316$ and $\sigma_0/\sigma_\infty = 0.5$. The triangles show the computed nodal values and the straight line is the distribution according to the rigid grains model.

matter being transported from the cavity walls becomes more localized. Since the rigid body separational velocity of the grains is decreasing as $(a/L)^{-3}$, the enhancement of the cavity growth rate due to this accommodation becomes more pronounced.

The numerical results obtained here for the cavity volumetric growth rate can be compared with the results of the approximate upper bound analysis of Edward and Ashby [10]. Their upper bound on the cavity volumetric growth rate takes the form

$$\frac{\dot{V}}{\epsilon_\infty a^3} \leqslant 2\pi\left(\frac{b^2}{a^2} - 1\right)\left[\left(\frac{1+P}{1-a^2/b^2}\right)^n - 1\right] \quad (63)$$

where

$$P = \frac{1}{10}\left(\frac{4L^3}{b^3}\right)^{2/n}$$

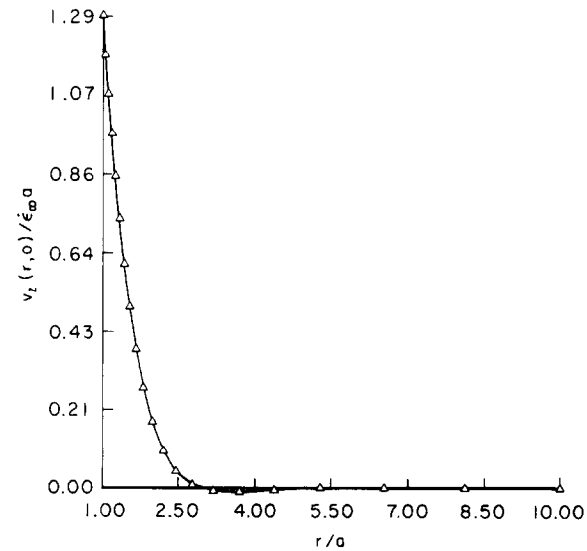

Fig. 7. The vertical velocity distribution (half the separational velocity of the grains) along the grain boundary for $a/b = 0.1$, $a/L = 1.0$ and $\sigma_0/\sigma_\infty = 0.5$. The triangles show the computed nodal values. Here, the straight line giving the distribution according to the rigid grains model essentially coincides with the horizontal axis on the scale of the figure.

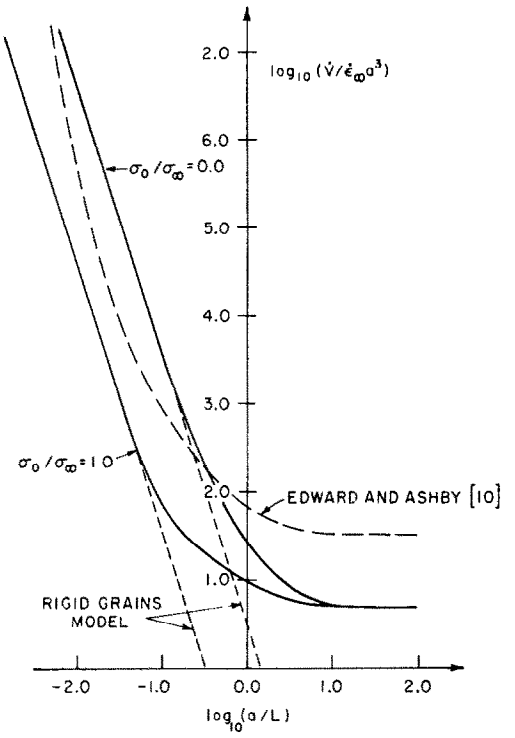

Fig. 8. Log-log (base 10) plot of the cavity volumetric growth rate versus a/L for $a/b = 0.1$, and for extreme values of the ratio of the classical sintering limit stress to applied stress, $\sigma_0/\sigma_\infty = 0.0$ and $\sigma_0/\sigma_\infty = 1.0$. For comparison purposes the predictions of the rigid-grains model and the upper bound analysis of Edward and Ashby [10] are also shown.

and in obtaining (63), Edward and Ashby [10] assume σ_0 negligible.

Figure 8 gives a log-log (base 10) plot of the computed normalized cavity volumetric growth rates versus a/L, for $a/b = 1/10$ and with $\sigma_0/\sigma_\infty = 0.0$ and 1.0. The numerical results, plotted from the values in Table 2, are extrapolated past $a/L = 10.0$ in Fig. 8. Also plotted in this figure is the right hand side of (63). In the power law creep dominated regime the upper bound of Edward and Ashby [10] is about a factor of six above the computed cavity growth rate. For example at $a/L = 10.0$, (63) gives an upper bound of 34.3 while the numerical values of $\dot{V}/\dot{\epsilon}_\infty a^3$ range from 5.34 for $\sigma_0/\sigma_\infty = 0.0$ to 5.10 for $\sigma_0/\sigma_\infty = 1.0$.

In the limit of essentially rigid grains behavior, a/L small or P large, (63) gives $\dot{V}/\dot{\epsilon}_\infty a^3 \sim (a/L)^{-6}$, whereas the rigid grains model, with which the numerical results coincide in this limit, gives $\dot{V}/\dot{\epsilon}_\infty a^3 \sim (a/L)^{-3}$. Thus, for sufficiently small a/L, approximately $a/L \sim 10^{-2.5}$ in Fig. 8, (63) also gives an upper bound. In this regime the cavity growth rate as given by the rigid grains model, presumed valid in this limit, is significantly below the upper bound (63).

For intermediate values of a/L, where the coupling between grain boundary diffusion and plastic creep flow is significant, the right hand side of (63) falls between the computed results for $\sigma_0/\sigma_\infty = 1.0$ and $\sigma_0/\sigma_\infty = 0.0$. Hence, (63) is not a true upper bound.

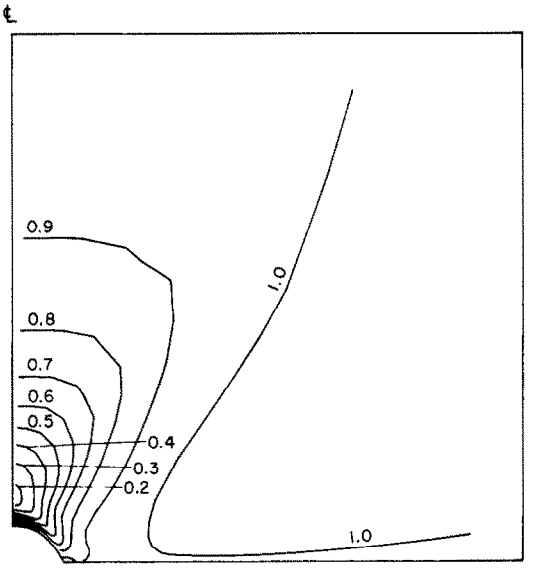

Fig. 9. Contours of constant effective creep strain rate, $\dot{E} = \dot{\epsilon}/\dot{\epsilon}_\infty$, for $a/b = 0.1$, $a/L = 0.316$ and $\sigma_0/\sigma_\infty = 0.5$.

As mentioned in the Introduction, the analysis of Edward and Ashby [10] is based on the concept, introduced by Beere and Speight [9], of the cavity being surrounded by a shell of effectively non-creeping material. To explore the appropriateness of this concept in light of the present numerical solutions, Figs 9 to 11 exhibit contours of constant effective creep strain rate for $a/b = 1/10$, $\sigma_0/\sigma_\infty = 0.5$ and $a/L = 0.316$, 1.0 and 3.16 respectively. In these figures, the contours are curves of constant effective creep strain rate normalized by the remote effective creep strain rate.

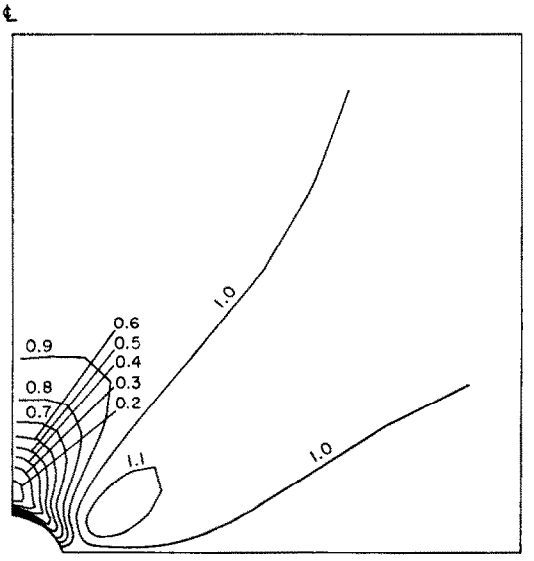

Fig. 10. Contours of constant effective creep strain rate, $\dot{E} = \dot{\epsilon}/\dot{\epsilon}_\infty$, for $a/b = 0.1$, $a/L = 1.0$ and $\sigma_0/\sigma_\infty = 0.5$.

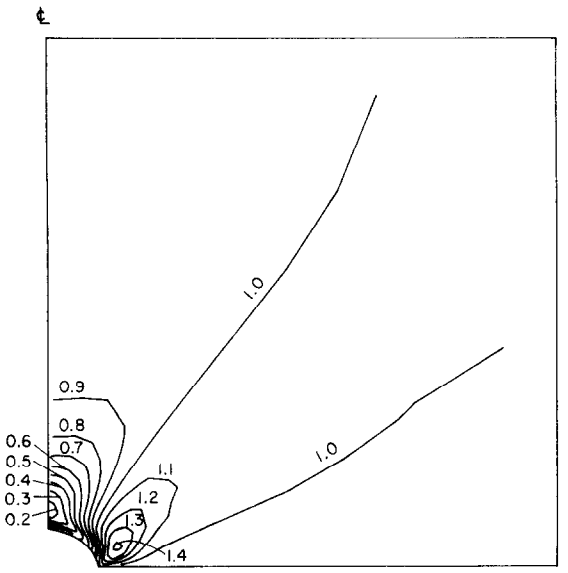

Fig. 11. Contours of constant effective creep strain rate, $\dot{E} = \dot{\epsilon}/\dot{\epsilon}_\infty$, for $a/b = 0.1$, $a/L = 3.16$ and $\sigma_0/\sigma_\infty = 0.5$.

In Fig. 9, where $a/L = 0.316$, the maximum effective creep strain rate occurs at the cavity along the axis of symmetry, and has a value of about $\dot{E} = 1.1$. Except for this small zone of plastic creep deformation, the cavity is surrounded by a diffusionally relaxed region, with the grain material outside this relaxed region deforming nearly homogenously, with the region bounded by $\dot{E} = 1.0$ being a plateau on which $1.0 \leq \dot{E} < 1.1$. For a smaller value of a/L than 0.316, the contours of $\dot{E}$ exhibit a similarly shaped, but larger, diffusionally relaxed region to that depicted in Fig. 9.

As a/L increases, in Figs. 10 and 11, the diffusionally relaxed zone moves up from the grain boundary and the plateau of effective creep strain rate becomes more peaked and propagates toward the cavity tip. Note also that the creep deformation zone along the cavity boundary near the axis of symmetry is relaxed.

In Figs. 5–11 we have plotted features of the numerical results for $a/b = 1/10$. Qualitatively similar features, although differing in detail, were observed for the other values of a/b considered.

As is evident from the results displayed so far, the numerical solution depend in a complex way on the parameter a/L. In contrast, the dependence of the cavity volumetric growth rate on σ_0/σ_∞ is surprisingly simple; the cavity volumetric growth rates displayed in Tables 2 to 5 are linear in σ_0/σ_∞. Of course, such linearity must emerge in the rigid grains limit, but there is no obvious reason (to us) why a linear relation should persist into the regime where the plastic creep flow effects are significant. As illustrated in Fig. 12, where each computed point is marked, the linear dependence of the cavity growth rate on σ_0/σ_∞ covers the range from $\sigma_0/\sigma_\infty = 0.0$ to the sintering limit at which $\dot{V}$ vanishes for $a/L = 0.316$ and 1.0. Denoting the value of σ_0/σ_∞ at the sintering limit by $(\sigma_0/\sigma_\infty)_s$, the rigid grains approximation gives

$$(\sigma_0/\sigma_\infty)_s = [1 - a^2/b^2]^{-1}. \tag{64}$$

Linear extrapolation of the values of $\dot{V}/\dot{\epsilon}_\infty a^3$ in Table 2 for $a/L = 0.01$, 0.0316 and 0.1 all give $(\sigma_0/\sigma_\infty)_s = 1.01$, in agreement with (64). However, from Fig. 12, $(\sigma_0/\sigma_\infty)_s = 1.10$ and 1.59 for $a/L = 0.316$ and 1.0 respectively.

Although here we do not pursue, in detail, an investigation of the dependence of the sintering limit on plastic creep flow, we note that a similar linear extrapolation, to that above, carried out for $a/L = 3.16$ with $(\sigma_0/\sigma_\infty) = 4.0$ and 4.5 gave positive cavity volumetric growth rates, thereby illustrating that the linear dependence of $\dot{V}/\dot{\epsilon}_\infty a^3$ exhibited in Tables 2 to 5 and Fig. 12 is not a general attribute of solutions of (46). Indeed, as remarked previously, in the limit of a/L large, solutions of (46) approach the pure power law creep solutions, for which $\dot{V}/\dot{\epsilon}_\infty a^3$ is positive and independent of σ_0/σ_∞.

These considerations show that in the presence of plastic creep flow the classical sintering limit of equation (64) is irrelevant if conditions are such that L is comparable to or smaller in size than a. Voids then continue to grow even when the applied stress is less than the classical limit.

7. ESTIMATE OF THE TIME TO RUPTURE

When fracture occurs by intergranular cavitation, the time to rupture t_r, and the steady-state creep rate, at a constant applied stress, $\dot{\epsilon}_{ss}$, are sometimes found

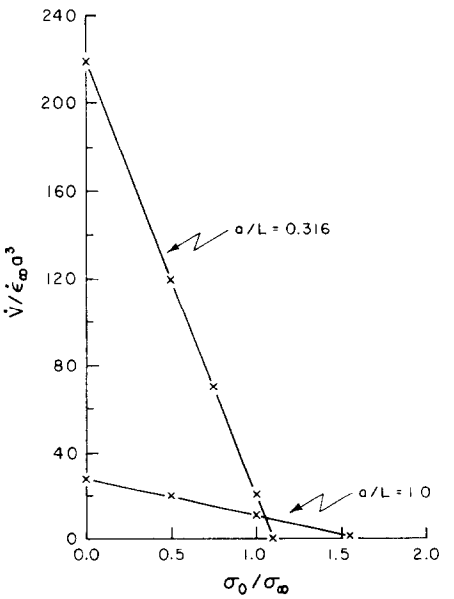

Fig. 12. Plot of the computed normalized cavity volumetric growth rate versus σ_0/σ_∞ for $a/b = 0.1$, $a/L = 0.316$ and $a/L = 1.0$.

experimentally to be related by the well-known Monkman–Grant [8] correlation

$$\dot{\epsilon}_{ss}\, t_r = \text{constant}. \tag{65}$$

Typically, $\dot{\epsilon}_{ss}t_r$ has a value in the range between 0.05 and 0.5.

The numerical results presented in the preceding section will be utilized to obtain an estimate of $\dot{\epsilon}_{ss}t_r$ under the assumption that the surface diffusion is sufficiently rapid to maintain the equilibrium spherical-caps cavity shape. We emphasize that the validity of this assumption, when plastic creep flow effects are significant, is an open question.

Here, we define the rupture time, t_r, as the time for a cavity to grow from an initial radius, a_i, to the limiting radius, b, at which there is coalescence. Thus, we neglect the contribution to the rupture time of the time required to nucleate the cavities, which, in practical cases (see Raj and Ashby [16]), can be significant.

Differentiating (4) with respect to time and rearranging terms gives

$$\dot{\epsilon}_{ss}t_r = \int_{a_i}^{b} \frac{4\pi h(\psi)a^{-1}\,da}{[\dot{V}/\dot{\epsilon}_{ss}a^3]} \tag{66}$$

where, here, $\dot{\epsilon}_{ss}$ is properly identified with the remotely imposed strain rate, $\dot{\epsilon}_\infty$, and the denominator on the right hand side of (66) is a function of the current values of a/b, a/L and σ_0/σ_∞ (here $\sigma = A\dot{\epsilon}_{ss}^{1/n}$).

Rather than directly evaluating the integral in (66), it proved convenient to adopt the following numerical procedure. The current time derivative of the cavity radius, $\dot{a}$, is written, from (4), as

$$\dot{a} = \frac{a\dot{\epsilon}_{ss}}{4\pi h(\psi)} \frac{\dot{V}}{\dot{\epsilon}_{ss}a^3}$$

$$= \frac{a\dot{\epsilon}_{ss}}{4\pi h(\psi)} F\left(\frac{a}{b}, \frac{a}{L}, \sigma_0/\sigma_\infty\right) \tag{67}$$

Here, $\dot{\epsilon}_{ss}$ is identified with $\dot{\epsilon}_\infty$ and the appropriate value of $F(a/b, a/L, \sigma_0/\sigma_\infty)$ is chosen by interpolating between the values given in Tables 2–5. First, for the current value of a/b a table analogous to Tables 2–5 is constructed. This table is constructed by linear interpolation of either $\dot{V}/\dot{\epsilon}_\infty a^3$ or $\dot{V}/\dot{V}_{RG}$, whichever has the smallest relative change (change in the entry divided by the minimum of the entries in the two of Tables 2–5 employed in the interpolation). Then for those entries for which $\dot{V}/\dot{V}_{RG}$ is interpolated, $\dot{V}/\dot{\epsilon}_\infty a^3$ is calculated by multiplying $\dot{V}/\dot{V}_{RG}$ by $\dot{V}_{RG}/\dot{\epsilon}_\infty a^3$ where $\dot{V}_{RG}$ is determined from (9). For example, if the current value of a/b is 0.15, the value of $\dot{V}/\dot{\epsilon}_\infty a^3$ entered in the table for $a/L = 0.1$ and $\sigma_0/\sigma_\infty = 1.0$ would be determined by linear interpolation of $\dot{V}/\dot{V}_{RG}$ between 1.62 and 1.06, and then multiplying the interpolated value (1.34) by the value of $\dot{V}_{RG}/\dot{\epsilon}_\infty a^3$ calculated, from (9), with $a/b = 0.15$, the value of $\dot{V}/\dot{\epsilon}_\infty a^3$ entered in the table for $a/L = 1.0$ and $\sigma_0/\sigma_\infty = 0.0$ would be determined by linearly interpolating between 27.3 and 27.6.

The second step consists of linearly interpolating between the two values of σ_0/σ_∞ to give $\dot{V}/\dot{\epsilon}_\infty a^3$, at the current values of a/b and σ_0/σ_∞, for $a/L = 0.01$, 0.0316---10.0. (For $a/L > 10.0$, it is assumed that the value of $\dot{V}/\dot{\epsilon}_\infty a^3$ at $\sigma_0/\sigma_\infty = 1.0$, $a/L = 10.0$ constitutes an adequate approximation to the plastic creep flow limit.) The third and final step employs linear interpolation of $\log_{10}(\dot{V}/\dot{\epsilon}_\infty a^3)$, considered as a function of $\log_{10}(a/L)$. Here, this logarithmic interpolation is employed, since as exhibited in Fig. 8, $\log_{10}(\dot{V}/\dot{\epsilon}_\infty a^3)$ is a rather slowly varying function of $\log_{10}(a/L)$ for which linear interpolation can be expected to be reasonably accurate.

The value of $\dot{a}$ at the current time, t, is then readily calculated from (67). The value of cavity radius, a, at $t + dt$ is given by $[a(t) + \dot{a}\,dt]$ where dt is chosen so that $[a(t) + \dot{a}\,dt]$ is equal to $1.01a$. Then, the values of a/b, a/L and, from (10), σ_0 are calculated and the whole procedure repeated. The calculation initiates at $a = a_i$ and terminates when $a = b$. In order to carry out the calculation for $a/b > 2/3$, the appropriate value of $\dot{V}/\dot{\epsilon}_\infty a^3$ is given by an extrapolation procedure analogous to the linear interpolation procedure described above. The final result is not particularly sensitive to the details of the extrapolation scheme employed, since typically, 85% or more of the rupture time has elapsed when $a/b = 2/3$, for the cases considered here.

The final result gives $\dot{\epsilon}_{ss}t_r$ as a function of b/L, a_i/b and $(\sigma_0/\sigma_\infty)_i$. Results for $\dot{\epsilon}_{ss}t_r$ as a function of b/L for various ratios of initial cavity radius to spacing with $(\sigma_0/\sigma_\infty)_i = 0.0$ and 1.0, are shown in Fig. 13. Also shown in this figure, for comparison purposes, are the predictions of the model of Edward and Ashby ([10] Fig. 9) for this case.

For small b/L, the cavity growth rate is purely diffusion controlled and, from (9), with which the numerical results agree (to within 1%), in this limit for $a_i/b = 1/10$,

$$\dot{\epsilon}_{ss}t_r = 3.03 \times 10^{-2}\left(\frac{b}{L}\right)^3 \quad \text{for} \quad (\sigma_0/\sigma_\infty)_i = 0.0$$

$$\dot{\epsilon}_{ss}t_r = 5.02 \times 10^{-2}\left(\frac{b}{L}\right)^3 \quad \text{for} \quad (\sigma_0/\sigma_\infty)_i = 1.0 \tag{68}$$

At the other limit, b/L large, the diffusional contribution to the cavity growth rate is negligible, $\dot{V}/\dot{\epsilon}_{ss}a^3$ is independent of $(\sigma_0/\sigma_\infty)_i$ and nearly constant over most of the lifetime. Approximating this constant by 5.2 and carrying out the integration in (66) gives,

$$\dot{\epsilon}_{ss}t_r \cong 3.4 \tag{69}$$

For intermediate values of a_i/b, the values of $\dot{\epsilon}_{ss}t_r$, at fixed b/L, depends somewhat on $(\sigma_0/\sigma_\infty)_i$; for example, for $b/L = 3.16$, $\dot{\epsilon}_{ss}t_r = 0.38$ and 0.52 for $(\sigma_0/\sigma_\infty)_i = 0.0$ and 1.0, respectively. However, as can be seen in Fig. 13, the value of $\dot{\epsilon}_{ss}t_r$ is a much more sensitive function of b/L than of $(\sigma_0/\sigma_\infty)_i$, at least for the parameter values considered here.

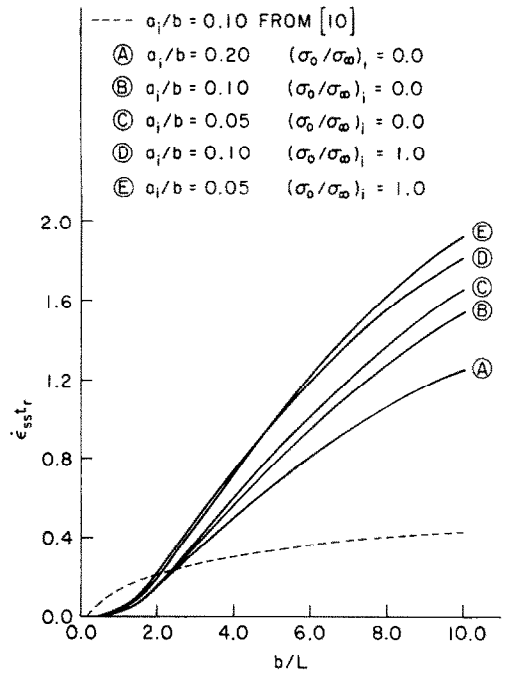

Fig. 13. Plots of the Monkman–Grant product $\dot{\epsilon}_{ss}t_r$, where $\dot{\epsilon}_{ss}$ is the remotely imposed strain rate (based on plastic dislocation creep only) and t_r is the time to coalescence, vs b/L for various values of the initial cavity radius to spacing ratio a_i/b and various ratios of the classical sintering limit stress to applied stress $(\sigma_0/\sigma_\infty)_i$.

The model of Edward and Ashby [10] underestimates the value of $\dot{\epsilon}_{ss}t_r$ in the regime where cavity growth takes place primarily by power law creep. This is consistent with the fact that their upper bound, as illustrated in Fig. 8, is about a factor of 6 greater than the numerical results in this regime. It should also be noted that the assumption, embodied in our calculation of the rupture time, as well as in that of Edward and Ashby [10], that the cavity retains its equilibrium spherical-caps shape is particularly questionnable in this regime. For $b/L \approx 2$ there is, as shown in Fig. 13, agreement between the predictions of the Edward and Ashby [10] model and the present results. For very small b/L, say $b/L < 10^{-1}$, the residual rupture time, due to pure diffusional growth, is underestimated by their model, since it gives a cavity growth rate that is greater than given by (9) in this limit, as discussed in reference to Fig. 8.

The results in Fig. 13 show that a Monkman–Grant correlation cannot be expected from considerations of cavity growth alone. Indeed, Miller [26] has recently emphasized the different stress dependencies for the growth rate of existing cavities, and for the total rupture time in αFe, attributing the difference to the time required for nucleation. However, in cases for which all or most of the lifetime to rupture involves cavity growth, the results in Fig. 13 suggest that values of the Monkman–Grant product in the representative range from approximately 0.05 to 0.5 will result for a wide range of b/L (from approximately 1 to 4) for essentially all ratios of initial cavity size to spacing and of applied stress to the classical sintering limit. Further, the term $\dot{\epsilon}_{ss}$ in Fig. 13 refers to the strain rate associated with plastic creep alone. Diffusional contributions to the overall steady creep rate become increasingly more important compared to plastic contributions at small values of b/L, and this will tend to make the actual value of the Monkman Grant product somewhat higher than what we show in Fig. 13 for small b/L.

8. SUMMARY AND CONCLUSIONS

1. It has been shown that plastic creep flow interacts with diffusional processes of grain boundary cavity growth. The principal effect is that creep deformability of the grains allows matter diffused from the cavity walls to be accommodated by local separations of the adjoining grains in the vicinity of the cavity (Figs. 2b and 5 to 7), thus shortening the effective diffusion path length and resulting in greater rates of cavity growth than would be the case if either grain boundary diffusion or plastic creep flow acted in isolation.

2. A quantitative analysis of the process has been based on a variational principle governing combined processes of plastic creep flow and grain boundary diffusion, employed as the basis of a finite-element numerical solution for the growth of a spherical-caps cavity of radius a, spaced at center-to-center distance $2b$ with neighboring cavities.

3. The resulting cavity growth rates are found to be greatly in excess of those based on the rigid grains (Hull–Rimmer) model, Tables 2 to 5 and Fig. 8, whenever the stress and temperature dependent parameter L is of a size comparable to or smaller than the cavity radius a.

4. Values of the parameter L are presented in Table 1 and suggest, e.g., that at $0.5\,T_m$ the coupling between plastic creep and diffusion will generally be significant at stresses of the order $10^{-3}\,\mu$ or higher, but not at stresses of the order $10^{-4}\,\mu$ or lower. L decreases in size with increasing stress and/or temperature.

5. The patterns of the Mises equivalent shear strain rate distribution presented in Figs. 9 to 11 do not support closely the concept of a non-deforming spherical zone adjoining the cavity and embedded in a cage of plastically deforming material, although more complexly shaped zones of effectively non-deforming material do result immediately above and below the cavity.

6. In the presence of overall plastic creep flow, cavities continue to grow (Fig. 12) even at applied stress levels which are somewhat less than the classical sintering limit. The effect is most pronounced for values of a/L of the order unity or larger.

7. Integration of the cavity growth rate equations leads to predictions of rupture times t_r based on growth alone (i.e., ignoring nucleation), which are

such that the Monkman–Grant product $\dot{\epsilon}_{ss}t_r$ varies with stress level and temperature, for a given initial cavity size a_i and half spacing b (Fig. 13).

8. The analysis is based on the assumption that surface diffusion is sufficiently rapid to retain a quasi-equilibrium type of spherical-caps cavity shape. The range of validity of this assumption will certainly be limited, especially in low-L cases for which rapid cavity growth is predicted. This is an important topic for further study. Also, elastic and transient creep behavior of the grains has been neglected. These are expected to be important following alterations of load level, although not for long-time sustained loading.

Acknowledgements—This study was supported by the U.S. Department of Energy under contract EY-76-02-3084.A001 with Brown University. We are grateful to Professor M. F. Ashby for helpful discussions and for the communication of materials data, and to Mr. A. Rubenstein for assistance in the preparation of Table 1.

REFERENCES

1. D. Hull and D. E. Rimmer, *Phil. Mag.* **4,** 673 (1959).
2. M. V. Speight and J. E. Harris, *Metal. Sci. J.* **1,** 83 (1967).
3. J. Weertman, *Scripta Metall.* **7,** 1129 (1973).
4. T-J. Chuang and J. R. Rice, *Acta Metall.* **23,** 425 (1973).
5. T-J. Chuang, K. I. Kagawa, J. R. Rice and L. B. Sills, *Acta Metall.* **27,** 265 (1979).
6. T-J. Chuang, Ph.D. Thesis, Brown University (1974).
7. V. Vitek, *Acta Metall.* **26,** (1978).
8. F. C. Monkman and N. J. Grant, *Proc. ASTM* **56,** 593 (1956).
9. W. Beere and M. V. Speight, *Metal Sci.* **4,** 172 (1978).
10. G. H. Edward and M. F. Ashby, *Acta Metall.* **27,** 1505 (1979).
11. J. R. Rice, *Time Dependent Fracture of Materials at Elevated Temperature* (edited by S. Wolf), p. 130, U.S. Department of Energy Report CONF 790236 UC-25, Germantown, Md. (June 1979).
12. J. Weertman, *Metall. Trans.* **5,** 1743 (1974).
13. J. W. Hancock, *Metal Sci.* **10,** 319 (1976).
14. B. Budiansky and R. J. O'Connell, *Int. J. Solids Struct.* **12,** 81 (1976).
15. J. R. Rice and T-J. Chuang, *J. Am. Ceram. Soc.* in press.
16. R. Raj and M. F. Ashby, *Acta Metall.* **23,** 653 (1975).
17. R. Raj, H. M. Shih and H. H. Johnson, *Scripta Metall.* **11,** 839 (1977).
18. H. J. Frost and M. F. Ashby, privately communicated compilation of high temperature creep and diffusion data (1979).
19. A. Needleman and C. F. Shih, *Comp. meth. appl. Mech. Engng* **15,** 223 (1978).
20. C. Herring, *Structure and Properties of Solid Surfaces* (edited by R. Gomer and C. S. Smith), Univ. of Chicago Press (1952).
21. C. Herring, *The Physics of Powder Metallurgy*, p. 143 (edited by W. E. Kingston), McGraw-Hill (1951).
22. M. F. Ashby, *Acta Metall.* **20,** 887 (1972).
23. S. H. Goods and W. D. Nix, *Acta Metall.* **26,** 739 (1978).
24. S. H. Goods, Ph.D. Thesis, Stanford University (1977).
25. R. Raj, *Acta Metall.* **26,** 341 (1978).
26. D. A. Miller, *Scripta Metall.* **13,** 595 (1979).